Biophysical Chemistry 7 (1978) 347–366

SCANNING MOLECULAR SIEVE CHROMATOGRAPHY OF INTERACTING PROTEIN SYSTEMS. SIMULATION OF LARGE ZONE BEHAVIOR FOR SELF-ASSOCIATING SOLUTES UNDERGOING RAPID CHEMICAL EQUILIBRATION UNDER KINETIC CONTROL ☆

Paul W. CHUN ‡ and Mark C.K. YANG ‡

Department of Biochemistry and Molecular Biology, College of Arts and Sciences, University of Florida, Gainesville, Florida 32610, USA

Received 17 January 1977
Revised manuscript received 1 September 1977

Theoretical large zone reaction boundaries for molecular sieve chromatography have been simulated by computer for a self-associating solute undergoing rapid chemical equilibration under kinetic control. These patterns show that the kinetically-controlled reaction rate between the mobile and stationary phases is the principal determinant of the elution boundary profile in molecular sieve chromatography. The overall chemical reaction rate in the mobile phase was found to have a much greater role in a rapidly equilibrating system than did the effect of axial dispersion within the gel matrix.

1. Introduction

In recent years the experimental study of interacting protein systems has depended largely upon development of useful theories for interpretation of data that can be obtained by a variety of physical techniques such as light scattering, osmotic pressure, sedimentation equilibrium experiments and molecular sieve chromatography.

Since the pioneering work of Gilbert in 1955 [1], all transport experiments to date have dealt with the assumption that chemical equilibrium between the interacting species is instantaneous. Recently, attention has focused on kinetically controlled associating systems in relation to the time of duration of experiments, in an attempt to evaluate the observed boundary profiles. As yet, however, no analytical solution of the transport flux equation has been achieved [1–24,34, 35].

Attempts have been made to establish the effect of the kinetic rate of chemical interaction for self-associating species in the ultracentrifuge [9,10,12,17–19, 22] by electrophoresis [10], counter current distribution [25] and molecular sieve chromatography [20,21, 23,26].

A numerical solution of the flow equation for the molecular sieve chromatographic transport of multicomponent, interacting species has been formulated without consideration of kinetic effects. The behavior of large zones undergoing transport, including translational and rotational diffusion of solute within a chromatographic column, has been investigated by computer simulation [13–16].

However, more recently, Halvorson and Ackers [23] have formulated the kinetic constants for isomerization using small zone elution chromatography. Zimmerman [20,21] extended this method to consider kinetically-controlled monomer–*n*-mer and three-species association, as perturbed by the axial dis-

☆ This work was supported by NSF Grant PCM 76-04367 and, in part, by General Research Support, College of Medicine and the University of Florida Computer Center. Portions of this paper were presented at the 61st annual meeting of Federation of American Society for Experimental Biology, (Fed. Proc. 36, 3073), Chicago, Illinois, 1977.

‡ Address correspondence to P.W. Chun, Department of Biochemistry and Molecular Biology, College of Medicine, Box J245 J.H.M.H.C., University of Florida, Gainesville, Florida 32610, USA.

‡ Department of Statistics, College of Arts and Sciences, University of Florida, Gainesville, Florida 32610, USA.

persion coefficient (translational and rotational diffusion of interacting solute) in molecular sieve chromatography, maintaining a constant ratio of the kinetic rate constants corresponding to the equilibrium state, at which values of these kinetically controlled rate constants the resulting boundary profiles approach instantaneous chemical equilibrium.

In order to define as precisely as possible the effect of kinetic control on the elution boundary shapes of molecular sieve chromatographic patterns, we have considered at great length the computer simulation of the interacting species distribution in the mobile phase alone. These results are compared with the distribution patterns showing the kinetic effects on species interaction between the mobile and stationary phases.

In this communication, we report on the computer simulation of the continuity for chromatographic transport [20] as applied to a self-associating protein system. This paper, therefore, considers not only the solute–solute interaction in the mobile phase that has come to be assumed as a common feature of all kinetically-controlled transport systems, but also examines the influence of the kinetic effect between the mobile and stationary phase on the elution boundary profiles in molecular sieve chromatography with respect to all chemically interacting species.

2. Basic quantities and theoretical considerations

In order to realistically simulate the boundary behavior of interacting solutes by scanning molecular sieve chromatography, it is a prerequisite to have a basic understanding of the numerical solution of the continuity equation.

A general continuity equation, shown here, has been derived for the exchange of solute between stationary and mobile phases with simultaneous axial dispersion [24,27,28].

$$\partial C/\partial t + (F/\xi)\partial C/\partial X = L\partial^2 C/\partial X^2 . \quad (1)$$

Here, J represents the solute flux per unit cross-sectional area in which the solute is distributed within the column. F is the flow rate of eluent in ml/s and L is the axial dispersion coefficient, and ξ is the partition cross section.

The total flux, J, in gel chromatography can be considered to be the sum of two fluxes: (1) a flux, J_p due to solute partitioning and volume flow, and (2) axial dispersion, J_L, a rotational and translational flux due to non-equilibrium flow of the system. The solute partitioning term is $J_p = FC/\xi$; the axial dispersion term, $J_L = -L(\partial C/\partial X)$. The total flux $(J_p + J_L)$ is written as

$$J = FC/\xi - L(\partial C/\partial X) . \quad (2)$$

This is the fundamental flow equation for solute transport on the column, analogous to the processes of ultracentrifugation and free boundary electrophoresis. The chromatographic transport equation (1) results from the substitution of J from eq. (2) into the general continuity equation for a uniform cross-section, applicable to transport processes of all kinds [29]

$$(\partial C/\partial t) = -(\partial J/\partial X) . \quad (3)$$

Eq. (2) is applicable to a single component system where a chemical reaction or chemical equilibration is absent. When a solute species i enters into a chemical reaction with this system, this equation must be written as follows

$$J_i' = FC_i'/\xi_i - L_i\partial C_i'/\partial X + r_i , \quad (4)$$

where $C' = C\xi$ and $C' = \Sigma_i C_i\xi_i$. C' is the concentration within the column, including excluded regions as related to the bulk solute concentration. r_i is the rate of production or consumption of the interacting species i by the chemical reaction. The solute flux relative to the column frame of reference is $J' = J\xi$.

Since the total J_T' is the sum of the fluxes of all species present, eq. (4) above becomes

$$J_T' = \sum_i J_i' = \sum_i FC_i'/\xi_i - \sum_i L_i\partial C_i'/\partial X + \sum_i r_i . \quad (5)$$

Considering the simulation of eq. (5) which contains kinetically-controlled rate terms $(\Sigma_i r_i)$, it should be noted that system parameters and chemical reaction rate in the mobile phase, as well as the rate terms between mobile and stationary phases, influence the elution profiles of the interaction boundaries. In previous computer simulation [20,21, 23] only the chemical reaction rate term in the mobile phase was considered, without including the effect of kinetic terms between the mobile and stationary phases.

Considering a case of rapid equilibration in the mobile phase alone, eq. (5) may be solved for the gradient average of the velocity terms, F/ξ_i, of the individual species with respect to the C_i'. The overall velocity, $V_T = F/\xi_T$, is expressed as [13,24]:

$$V_T = F/\xi_T = \sum_i \frac{F}{\xi_i} K_i (C_1')^i \Big/ \sum_i K_i' (C_1')^i \qquad (6)$$

$$\xi_T = \sum_i \xi_i C_i \Big/ \sum_i C_i ,$$

where $C_i' = K_i'(C_1')^i$ and $K_i' = K_i \xi_i / (\xi_1)^i$. For self-associating solutes in which a reversible equilibrium is maintained during the course of the transport experiment, the concentration in free solution of each species i is given by $C_i = K_i C_1^i$.

Similarly, eq. (5) gives gradient average quantities.

$$L_T = \sum_i i L_i K_i' (C_1')^{i-1} \Big/ \sum_i i K_i' (C_1')^{i-1} . \qquad (7)$$

It should be noted that although K_i' is not a true equilibrium constant for the chemical reaction, it has the property of defining the relationship between C_i' and C_1' at each point in the column. The column equilibrium coefficient, K_i', contains the system parameters of ξ_i and ξ_T and the reaction stoichiometry, i, as well as the equilibrium constant K, where ξ_T is the weight average quantity of the self-associating solute species.

In our computer simulation, the following chemical equilibrium was considered.

$$i\mathrm{A}_1^* \underset{k_{ji}}{\overset{k_{ij}}{\rightleftharpoons}} \mathrm{A}_i^* . \qquad (8)$$

The component parameters considered apply to chemical equilibration in the mobile phase and equilibration between the mobile and stationary phases. Hence, the flux equation in the mobile phase is expressed as:

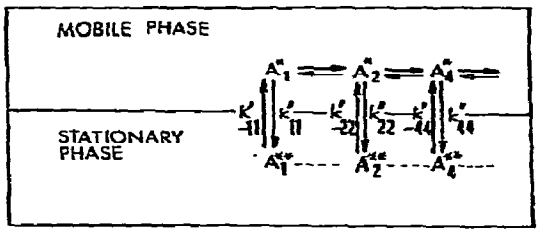

A simplified model for solute association in the mobile and stationary phases in the gel column.

$$\frac{\partial C_i^*}{\partial t} = L_i \frac{\partial^2 C_i^*}{\partial X^2} - \frac{F}{\xi_i} \frac{\partial C_i^*}{\partial X} \qquad (9)$$

$$- \sum_{j \neq i} k_{ij} (C_i^*)^j + \sum_{j \neq i} k_{ji} (C_j^*)^i - k_{-ii} C_i^* + k_{ii} C_i^{**} ,$$

where k_{ij} is the chemical reaction rate from species i to j as shown in eq. (8), and C_i^* is the concentration of species i. The

$$- \sum_{j \neq i} k_{ij} (C_i^*)^j + \sum_{j \neq i} k_{ji} (C_j^*)^i$$

term represents a rapid local equilibration rate in the mobile phase and $[-k_{-ii} C_i^* + k_{ii} C_i^{**}]$ represents the rate of equilibration between the mobile and stationary phases, where k_{ii} is the rate of reverse equilibration from the gel matrix to the mobile phase, and k_{-ii} is the rate of forward permeation from the mobile phase into the gel matrix. In eq. (9), it is apparent that no chemical reaction takes place or the system exhibits ideal behavior when k_{ij} becomes zero or infinity. Hence where $k_{ij} = 0$, only the A_i^* species is apparent; when $k_{ij} = \infty$, only A_j^* is present in the boundary profile.

Here we consider the solute partitioning process where k_{ii} or k_{-ii} between the mobile and stationary phase is either slow or rapid. In the former case, the boundary profile will show both the A_i^* and A_j^* associating species. In the latter case, only the distribution of the species A_i^* or A_j^* will appear in the boundary profile, i.e.

$$i\mathrm{A}^* \underset{k_{ji}}{\overset{k_{ij}}{\rightleftharpoons}} \mathrm{A}_i^* \quad \text{or} \quad j\mathrm{A}_{i-j}^* \rightleftharpoons \mathrm{A}_i^* ,$$

$$\mathrm{A}^* + \mathrm{A}_{j-1}^* \underset{k_{ji}}{\overset{k_{ij}}{\rightleftharpoons}} \mathrm{A}_j^* \quad \text{where } i = j - 1 . \qquad (8b)$$

Since the A^* species is present in excess, this reaction scheme is assumed to be pseudo first order kinetics. In our studies, we assumed that A^{**}, the concentration of the stationary phase, contributes less significantly to binding to the gel matrix (A^{**} + gel $\rightleftharpoons$ gel – A^{**}) than to the axial dispersion coefficient which is related to particle size, geometry and random variation in particle gel packing [24].

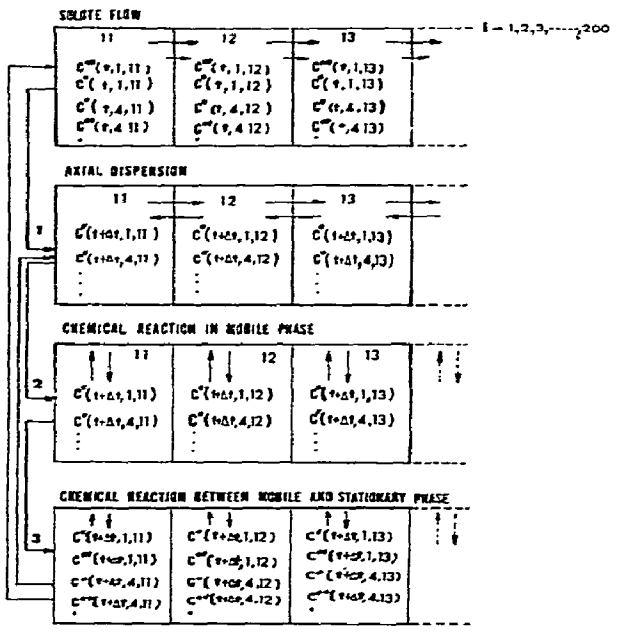

Fig. 1. Flow diagram for the computer simulation of a self-associating solute in scanning molecular sieve chromatography. Step 0 is solute flow; Step 1, axial dispersion; Step 2, chemical reaction in mobile phase; Step 3, chemical reaction between mobile and stationary phases. For a single component system, steps 0 and 1 are simulated. For two-species association (monomer–tetramer association) shown here, all four steps must be simulated. In three-species association (monomer–tetramer–octamer), each frame would contain three components. In the simulation procedure, the concentration term as a function of time must be determined for each frame of the flow diagram. Our computer program simulated such data for 200 frames.

3. Simulation procedures for large-zone boundary profiles

Our computer simulation procedure is based on the continuity equation (9), involving a finite difference approximation of Fick's second law by a method similar to that developed by Vink [30] and Cox [6,4].

The gel column (100 mm) was divided for convenience into n_x-frames of boxed compartments (2 mm) by $(n_x + 1)$ equally-spaced boundaries of the square cell, as shown in the schematic diagram of fig. 1. The total solute flow time was divided into $(n_t + 1)$ intervals of Δt. Equally-spaced compartments along the axis of the gel column were enclosed by the boundaries i and $(i + 1)$ where the interval between boundaries is designated ΔX. In step 1, (fig. 1), solute flows into each compartment from $(i - 1)$ over a time interval of $(t + \Delta t)$.

Each compartment of the three steps actually consists of both mobile and stationary phases, for which the continuity expressions for two-species association (monomer–tetramer association in this case) may be written as

$$\frac{\partial C_1^*}{\partial t} = L_1 \frac{\partial^2 C_1^*}{\partial X^2} - \frac{F}{\xi_1}\frac{\partial C_1^*}{\partial X}$$

$$-k_{14}(C_1^*)^4 + k_{41}C_4^* - k_{-11}C_1^* + k_{11}C_1^{**}\,, \qquad (13)$$

$$\frac{\partial C_4^*}{\partial t} = L_4 \frac{\partial^2 C_4^*}{\partial X^2} - \frac{F}{\xi_4}\frac{\partial C_4^*}{\partial X}$$

$$-k_{41}(C_4^*) + k_{14}(C_1^*)^4 - k_{-44}C_4^* + k_{44}C_4^{**}\,,$$

where C_1^* and C_4^* are the concentrations of solute species monomer and tetramer to be considered in the mobile phase, i.e.

$$A_1^* \underset{k_{41}}{\overset{k_{14}}{\rightleftharpoons}} A_4^*\,, \qquad (14)$$

where C_1^{**} and C_4^{**} are the concentration of solute in stationary phase with k_{ii} or k_{-ii} as defined in the diagram. Note that the total concentration $C_{Ti} = C_i^* + C_i^{**}$ and $C_i' = C_{Ti}\xi_i$.

The reverse and forward equilibration rate constants of species k_{11} and k_{-11} for monomer and k_{44} and k_{-44} for tetramer have their usual significance in the mobile phase, dictating the finite rate of equilibration or local equilibration rate wich will determine the boundary profiles of the system as whole. Thus, the rate of k_{ii} and k_{-ii} between mobile and stationary phases, as shown in fig. 1, becomes

$$\partial C_1^{**}/\partial t = -k_{11}C_1^{**} + k_{-11}C_1^*\,,$$

$$\partial C_4^{**}/\partial t = -k_{44}C_4^{**} + k_{44}C_4^*\,. \qquad (15)$$

This expression then, describes the stationary phase much as its counterpart, eq. (9), describes the mobile phase.

Letting $C_{1(t)}^*$ equal the concentration of monomer in the mobile phase at time t, solving eq. (15) for $C_{i(t+\Delta t)}^*$ yields $C_{i(t)}^*$ and $C_{i(t)}^{**}$ at t.

$$C^{**}_{i(t+\Delta t)} = \left\{ \frac{1}{(k_{ii} + k_{-ii})} [k_{ii} C^{**}_{i(t)} - k_{-ii} C^{*}_{i(t)}] \right.$$
$$\times \exp\{-(k_{ii} + k_{-ii})\Delta t\}$$
$$\left. + \frac{k_{-ii}}{k_{ii} + k_{-ii}} (C^{**}_{i(t)} + C^{*}_{i(t)}) \right\}, \quad i = 1, 2, \ldots \qquad (16)$$

The concentration of $C^{**}_{1(t+\Delta t)}$ is

$$C^{**}_{1(t+\Delta t)} = \left\{ \frac{1}{(k_{11} + k_{-11})} [k_{11} C^{**}_{1(t)} - k_{-11} C^{*}_{1(t)}] \right.$$
$$\times \exp\{-(k_{11} + k_{-11})\Delta t\}$$
$$\left. + \frac{k_{-11}}{(k_{11} + k_{-11})} (C^{**}_{1(t)} + C^{*}_{1(t)}) \right\}. \qquad (17)$$

Assuming that C^{*}_{1} is constant between $t = 0$ and Δt, then, for the tetramer,

$$C^{**}_{4(t+\Delta t)} = \left\{ \frac{1}{(k_{44} + k_{-44})} [k_{44} C^{**}_{1(t)} - k_{-44} C^{*}_{4(t)}] \right.$$
$$\times \exp\{-(k_{44} + k_{-44})\Delta t\}$$
$$\left. + \frac{k_{-44}}{(k_{44} + k_{-44})} (C^{**}_{4(t)} + C^{*}_{4(t)}) \right\}. \qquad (18)$$

In this case, all k_{ii} or k_{-il} are expressed in reciprocal minutes. The schematics of the individual compartments (as shown in fig. 1) may be considered. Since the concentration of species j of compartment i, at time t, is $C^{*}(t, j, i)$, then a change in concentration in compartment i of step 1 of this scheme is expressed as:

$$\Delta C^{*} = C^{*}_{(t+\Delta t, j, i)} - C^{*}_{(t, j, i)}. \qquad (19)$$

The total concentration C^{*} at $t + \Delta t$ is therefore $C^{*} = \Sigma_j C^{*}_{(t+\Delta t, j, i)} - C^{*}_{(t, j, i)}$ where $C^{*}_{(t, j, i)}$ denotes the concentration of species j of compartment i at the time t in the mobile phase. When describing the total concentration of solute species undergoing translational and rotational diffusion within the column, this equation may be written as:

$$C^{*}_{(t+\Delta t, j, i)} = C^{*}_{(t, j, i)} - \frac{L_j \{2C^{*}_{(t, j, i)} - C^{*}_{(t, j, i-1)} - C^{*}_{(t, j, i+1)}\}}{\Delta X^2 A / \Delta t}. \qquad (20)$$

Rearrangement of eq. (20) yields

$$\Delta C^{*} = -\frac{L_j \Delta t \{C^{*}_{(t, j, i+1)} + C^{*}_{(t, j, i-1)} - 2C^{*}_{(t, j, i)}\}}{A \Delta X^2} \qquad (21)$$

where L_j is the axial dispersion coefficient of species j and A is the cross-sectional area of the column. $C^{*}_{(t+\Delta t, j, i)}$, the concentration of species j in frame i at the time $(t + \Delta t)$ before proceeding to step 2 of fig. 1 where axial dispersion occurs is expressed as $C^{*} = C^{*}_{j} + [C^{*} - C^{*}_{j}]$. $C^{*}_{j} = C^{*}_{(t, j, i)}$ at the time interval t and $C^{*} = C^{*}_{(t+\Delta t, j, i)}$. Eq. (21) may be rewritten as follows:

$$C^{*} = C^{*}_{j} - L_j (\Delta^2 C^{*}_{i} / \Delta X^2)(\Delta t / A) \qquad (22)$$

obeying Fick's second law where $(\partial C / \partial t) = D(\partial^2 C / \partial X^2)$ [37].

In the case of monomer–tetramer association as is shown in fig. 1, the concentrations of monomer, $C^{*}_{1(t+\Delta t)}$, and tetramer, $C^{*}_{4(t+\Delta t)}$, in the mobile phase of steps 1 and 2 reach an instantaneous equilibrium and can be computed from eqs. (17) and (18). Thus, the total concentration of species j in compartment i is

$$C_{T(t+\Delta t, j, i)} = C^{*}_{(t+\Delta t, j, i)} + C^{**}_{(t+\Delta t, j, i)} \qquad (23)$$

where C^{**} is the concentration of the jth species in the stationary phase. The equilibrium concentration for the jth species at $(t + \Delta t)$ in compartment i of step 3 is denoted by $C^{*}_{(t+\Delta t\, j, i)}$. Hence, the apparent equilibrium constant K_{app} may be expressed in terms of C_{Ti}, i.e.

$$K_{app} = (C_{T4} / C^{4}_{T1}) = (C^{*}_{4} + C_{4}{}^{**}) / C^{*}_{1} + C^{**}_{1})^4 \qquad (24)$$

Following completion of these computations, steps 2 and 3 are repeated before returning to consider compartment $(i + 1)$ in step 1. Repetition of steps 2 and 3 takes into consideration the remaining fractions of the interecting species which were not involved in the chemical reaction and may be expressed as $C^{*}_{(t+\Delta t\, j, i)}$. The concentration after step 3 which must revert back to steps i and the initial step may be expressed as $C^{*}_{(t+\Delta t\, j, i)}$ and $C^{**}_{(t+\Delta t\, j, i)}$.

The initial concentration distribution which is considered in each frame of the scheme in fig. 1, is specifield by eqs. (17), (18), and (21). Once the calculations for a full cycle have been completed, the concentration for the next cycle becomes

$$\begin{aligned} &C^{*}_{(t+\Delta t, j, i)} \quad \text{steps 1, 2, 3} \\ &C^{*}_{(t+\Delta t, j, i+m_j)} \quad \text{step 0 (initial step)} \end{aligned} \qquad (25)$$

where m_j is the shift of frame by the species j.

This complete cycle will yield in turn, the next concentration expressions

$$C^*_{(t+2\Delta t,j,i')} \quad \text{step 1}$$

$$C^*_{(t+2\Delta t,j,i')} \quad \text{step 2} \qquad (26)$$

$$C^*_{(t+2\Delta t,j,i')} \quad \text{step 3}$$

where $i' = (i + m_j)$. After each successive instance of m-axial dispersion in step 1 and chemical reaction in step 2 and 3, the process always returns to solute flow. The shift to the next compartment $(i + m_j)$ occurs according to the solute flow rates of the interacting species, where m_j is defined such that $(Fm_j\Delta t)$ will produce an integer compartment shift for all species present in the system. This manipulation is similar to that proposed by Cox [4—7], and enables us to determine concentration as a function of column length, varying the flow time. Large zone profiles are obtained by taking the derivatives of the concentration with respect to column length at various flow times.

To check the validity of our simulation procedure in relation to other published data, a comparison between the theoretical and numerical simulation of a mono-dispersed system was made using the Halvorson and Ackers [31] procedure based on a gaussian distribution curve of the leading edges of the boundary. Here,

$$C_{(x,v)} = \tfrac{1}{2}C_0 \operatorname{erfc}\{\phi/[4L_vV)^{1/2}]\} \qquad (27)$$

where $L_v = L/F$, the experimentally obtainable axial dispersion coefficient, and $\phi = X - (Ft/\xi A)$, the new position coordinate describing the peak of the profile within the column. $X = \bar{V}/\xi A$, where $\bar{V}$ is the distribution volume, and V is the volume of solvent passed through the column at a constant flow rate F (see table 1).

Single components, monomer and tetramer in this case, could be numerically compared using our computer program, considering only solute flow and axial dispersion (steps 0 and 1 of fig. 1), for a single component in each frame of the scheme.

The simulation methods to be compared were incorporated into programs written in Fortran dialect, and the computation done on an IBM 370 computer. Concentration gradients (10000 dc'/dx) were plotted with a Gould plotter as a function of the x distance coordinate, varying the flow time and the effective rate of equilibration between mobile and stationary phases.

Table 1
System parameters used in simulation (held constant) [13]

column length, l	10 cm
column cross-sectional area, A	1.0 cm^2
Sephadex gel	G200R
flow rate, F	1.2 ml/h
α, void volume/ℓ	0.295
β, internal volume/ℓ	0.670
initial concentration, C_0	0.1 mg/ml
qd^2	5.4×10^{-6} cm^2

q is a gel particle-packing factor, d is the gel particle diameter. A is the column cross-sectional area. $\xi_i = \alpha + \beta\sigma_i$.

4. Results and discussion

Theoretical and numerical comparison of single components (monomer and tetramer).

The time-course dependent theoretical and numerical comparison of non-interacting single components, monomer and tetramer, based on eq. (27), is shown in fig. 2. Simulation in both figs. 2a and 2b was done on Sephadex G200R gel at a flow rate of 1.2 ml/h. The diameter of the monomer is 17.5 Å, that of the tetramer being 30 Å. The dark areas of these time-course dependent boundary profiles indicate that the theoretical and numerical simulations are virtually identical, with the two profiles for a single component system directly overlapping. In numerical simulations of the boundary profiles of the monomer and tetramer, only the effects of solute flow and translational and rotational diffusion are considered, as determined from the scheme described in fig. 1. No chemical reaction is assumed to take place in steps 2 or 3 of the flow diagram. For proper comparison of the two sets of theoretical and numerical data in terms of the distance coordinate, the running times for experiments at the two flow rates were simulated to maintain a constant flow throughout the experiment. The axial dispersion coefficients of monomer and tetramer used in this simulation were $L_1 = 3.61 \times 10^{-4}$ cm^2/min and $L_4 = 4.86 \times 10^{-4}$ cm^2/min, respectively. The simulated gradients are gaussian and symmetrical, and the degree of deviation is negligible. The close correla-

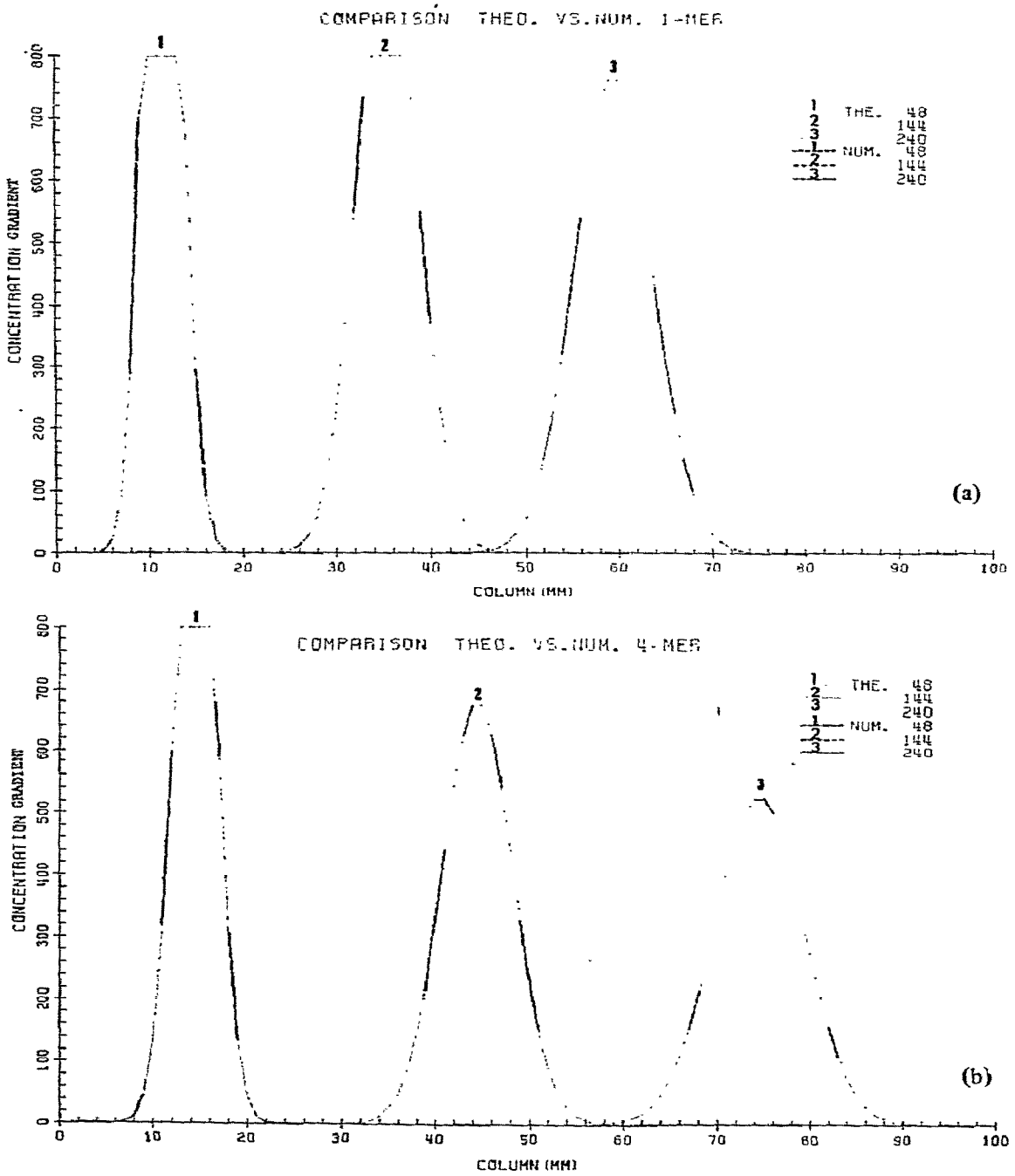

Fig. 2a, b. Theoretical and numerical comparison of non-interacting single components, (a) monomer and (b) tetramer. Concentration gradient (dc'/dx) × 10 000, as a function of the distance coordinate, x, varying the flow time. Flow rate, F = 1.2 ml/h, times are (1) 48 min, (2) 144 min, (3) 240 min, on Sephadex G200R (regular). Axial dispersion coefficients, $L_1 = 3.61 \times 10^{-4}$ cm²/min, $L_4 = 4.86 \times 10^{-4}$ cm²/min, $qd^2 = 5.4 \times 10^{-6}$ cm², $\alpha = 0.295$, $\beta = 0.67$, molecular radius of tetramer = 30 Å. Note the variation between theoretical and numerical calculations (—— numerical, --- theoretical).

tion of the profiles under these conditions is a good indicator of the effectiveness of our program in simulating transport boundary behavior.

4.1. The effect of kinetically-controlled interaction rates in the mobile phase

All simulations were carried out to describe the large zone boundary undergoing rapid chemical equilibration, using the simulation parameters described by Zimmerman and Ackers [13–16] (see table 1). The self-associating solute is assumed to be a monomer with a molecular radius of 18.9 Å, which corresponds approximately to a molecular weight of 17 000 daltons and a diffusion coefficient, D_{20w}, of 11.3 × 10^{-7} cm^2/s. The monomer is further assumed to form a dimer with a molecular radius of 23.8 Å and a diffusion coefficient of 8.97 × 10^{-7} cm^2/s. We assume that system parameters such as L, F, ξ and A are independent of the column length, X, time, t, and initial concentration, C as shown in table 1. In this case, the continuity expression (13) assumes that the establishment of differential diffusional equilibration is quite rapid between the mobile and stationary phases of every local region of the column bed. Hence, in rapidly reversible chemical equilibration, the solute profile is characteristic of the equilibrium composition of the mobile phase.

There are four cases of interest in the mobile phase which we have considered relative to the kinetically-controlled rate of chemical equilibration, i.e. the first three steps of the flow diagram in fig. 1 (steps 0, 1 and 2) where the boundary profile is under kinetic control.

Case (1) $k_{21} = 0.0\ \text{min}^{-1}$, $k_{12} = 0.1\ \text{min}^{-1}$

Case (2) $k_{21} = 0.005\ \text{min}^{-1}$, $k_{12} = 0.005\ K_2 (\text{min}^{-1})$

Case (3) $k_{21} = 0.05\ \text{min}^{-1}$, $k_{12} = 0.05\ K_2\ (\text{min}^{-1})$

Case (4) $k_{21} \geqslant 0.5\ \text{min}^{-1}$, $k_{12} \geqslant 0.5\ K_2\ (\text{min}^{-1})$ (28)

where $K_2 = C_2^*/(C_1^*)^2 = k_{12}/k_{21}$. K_i values are shown in tables 2 and 3, maintaining respective weight fractions of monomer.

In case (1), $k_{ij} = 0$, the chromatographic profile is that of a single solute of non-interacting species.

Table 2
System parameters in simulation

n-mer	σ_i	L_i(cm^2/min)	ξ_i
monomer	0.754	3.61×10^{-4}	0.80
dimer	0.634	4.00×10^{-4}	0.72
tetramer	0.515	4.86×10^{-4}	0.64
octamer	0.355	7.10×10^{-4}	0.533

Cases (2) and (3) fall into the category of rapid chemical equilibration. Case (4) represents a system undergoing such rapid equilibration in the mobile phase that no kinetic effect may be detected in the boundary profile when $k_{ij} > 0.5\ \text{min}^{-1}$. This is in contrast to cases (2) or (3), where the peak heights representing the finite equilibration rate are clearly distinguishable. These findings are consistent with results reported by Zimmerman [20].

As shown in figs. 3a and 3b, the maximum peak position in the gradient curve for a system undergoing monomer–dimer association is seen to shift toward higher values of a given distance coordinate with decreasing kinetically-controlled rates of equilibration, accompanied by a slight variation in the position of the trailing boundary. The sharpening of the boundary, therefore, is noticeably influenced by the kinetically-controlled rate of reaction [20,21].

The position and shape of the unimodel solute boundaries in the case of monomer–dimer association are shown in fig. 3. The weight fraction of monomer,

Table 3
Equilibrium constants and weight fractions of monomer

Monomer–dimer	Equilibrium constants K_2 (ml/mg)	Monomer–tetramer	Equilibrium constants K_4 (ml/mg)
90%–10%	1.2345	90%–10%	1.52×10^2
75%–25%	4.4440	75%–25%	7.90×10^2
50%–50%	20.000	50%–50%	8.00×10^3
25%–75%	120.00	25%–75%	1.92×10^5
10%–90%	900.00	10%–90%	9.00×10^6

Monomer–tetramer–octamer	Equilibrium constants	
	K_4 (ml/mg)	K_8 (ml/mg)
10% – 10% – 80%	1.0×10^6	8.0×10^{14}
5% – 15% – 80%	2.4×10^7	2.05×10^{17}
3% – 7% – 90%	8.64×10^7	1.37×10^{19}

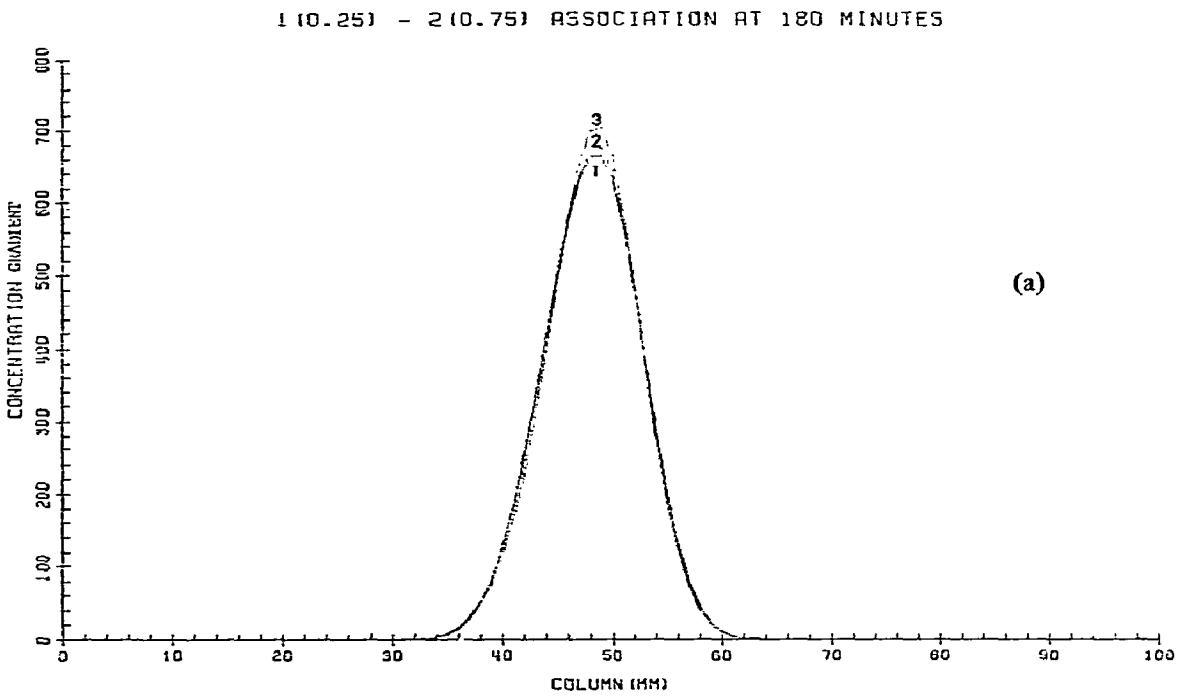
1 (0.25) - 2 (0.75) ASSOCIATION AT 180 MINUTES
CONCENTRATION GRADIENT
COLUMN (MM)
3
2
1
(a)

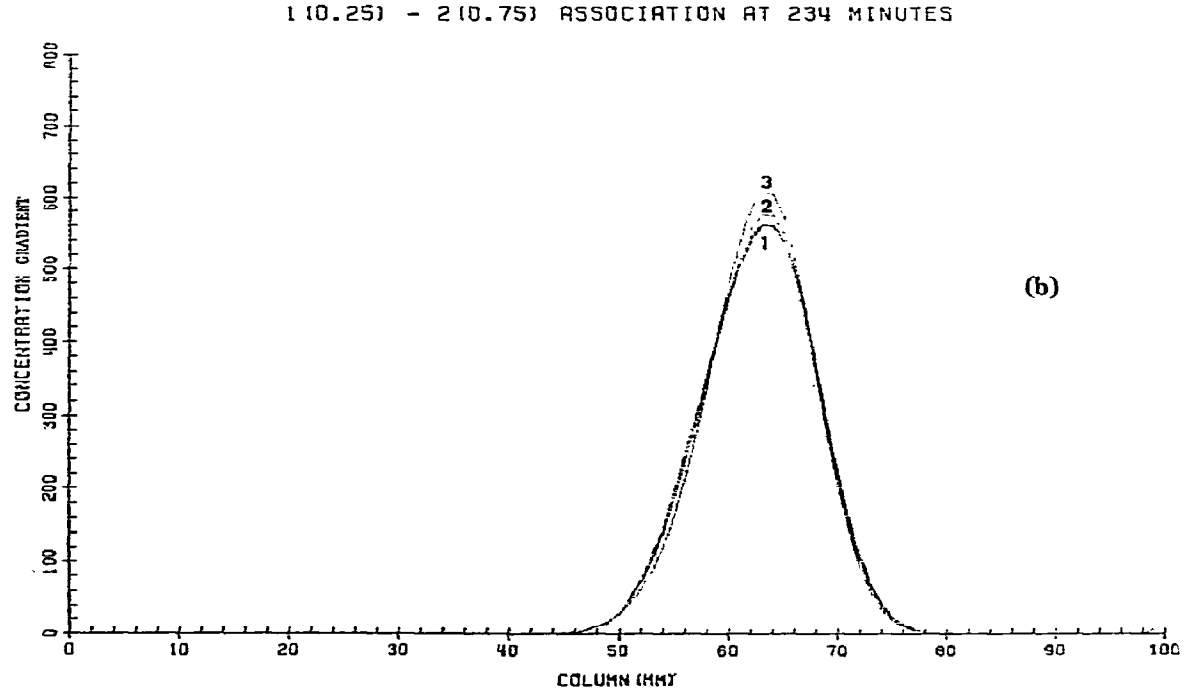
1 (0.25) - 2 (0.75) ASSOCIATION AT 234 MINUTES
CONCENTRATION GRADIENT
COLUMN (MM)
3
2
1
(b)

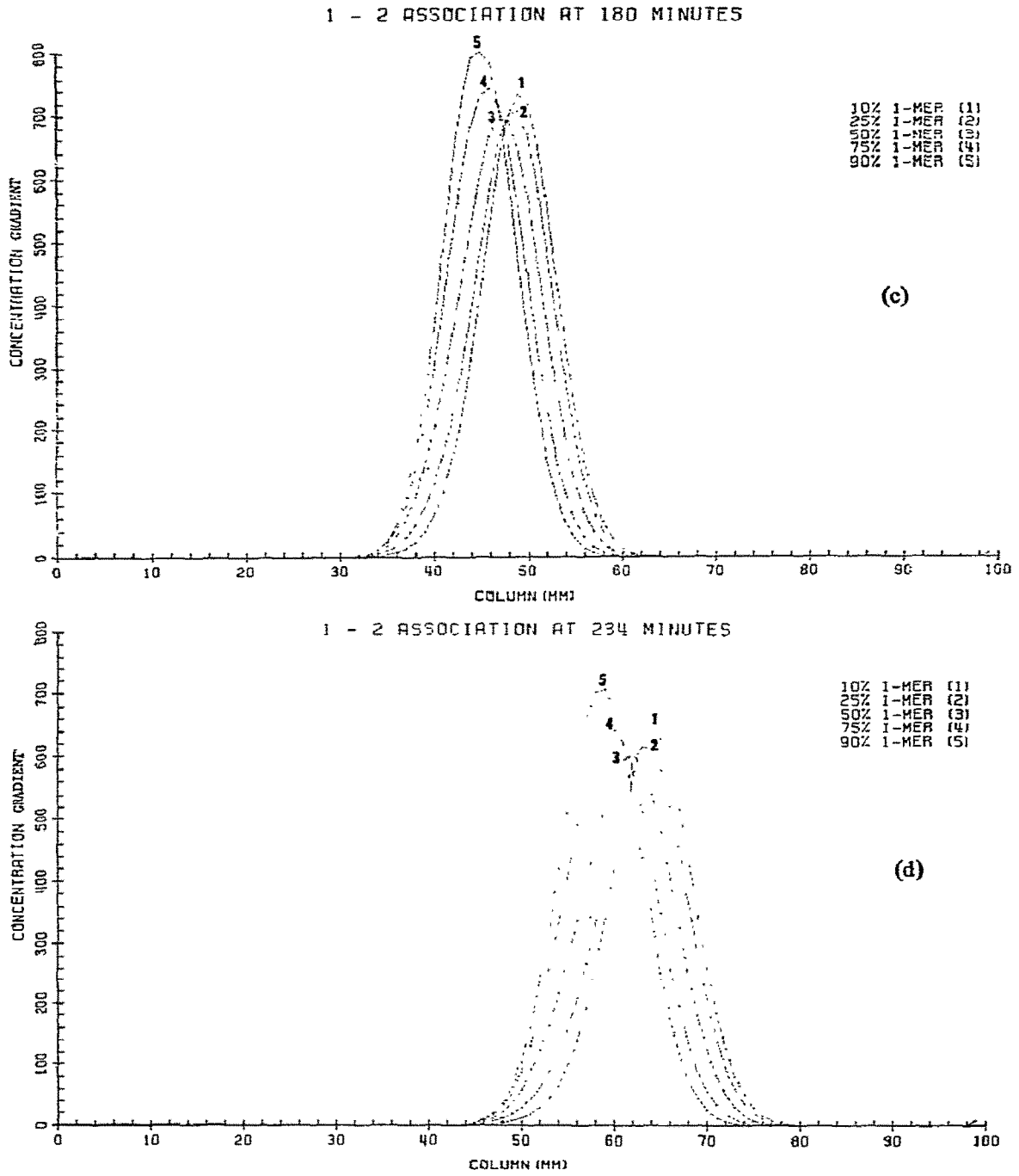

Fig. 3a, b, c, d. Effect of kinetically-controlled interaction boundaries of monomer–dimer system as a function of flow time in the mobile phase simulation of monomer–dimer equilibria of $f_1 = 0.25$ and $f_2 = 0.75$ at 180 min and 235 min. The column cross-sectional area is 1 cm^2. Flow rate is 1.2 ml/h. The monomer has a molecular radius of 18.9 A, corresponding to an approximate molecular weight of 17 000 daltons. The solute is initially present as a step function, $x = 0$, $t = 0$, and the loading concentration of the mobile phase within the column is 0.1 mg/ml. Equilibrium constants are given in table 3. (a) at 180 min. 1. $\kappa_{21} = 0.0$, 2. $k_{21} = 0.005$ min^{-1}, 3. $k_{21} > 0.5$ min^{-1}. (b) at 234 min. 1. $k_{12} = 0.0$, 2. $k_{12} = 0.005$ K_2 (min^{-1}), 3. $k_{12} > 0.5$ K_2 (min^{-1}). (c) 1-2 association at 180 min. 1. 10% monomer, 2. 25% monomer, 3. 50% monomer, 4. 75% monomer, 5. 90% monomer. (d) 1-2 association

$C_1^*/C_T^* = f_1^*$, is 0.25, and of dimer, $C_2^*/C_T^* = f_2^*$, is 0.75 at 180 min and 230 min intervals. The total concentration, C_T, within the column, is the same for all profiles and can be quantitatively expressed as:

$$C_T = C_1\xi_1 + C_2\xi_2, \tag{29}$$

where $C_i = C_i^* + C_i^{**}$ and ξ_1 and ξ_2 are assumed to be constant.

The maximum peak position in the gradient curve is seen to shift with variations in the composition of the weight fractions of monomer based on table 3, as seen in figs. 3c and 3d. In the case shown, the kinetic rate, $k_{ij} \geqslant 0.5$ min^{-1}, when k_{ij} is in the range of 0.005 min^{-1} and 0.05 min^{-1}. The maximum height of the peak position is reduced, accompanied by a slight shift in the trailing boundary, varying the composition of the weight fraction of monomer.

Zimmerman and Ackers [13–15] have demonstrated that the primary effect of increasing solute flow is to sharpen the reaction boundary, while exactly the opposite is observed in large zone experiments. If the leading boundary continuously feeds the dimer species into the solvent layer, then it is difficult to determine from elution profiles alone whether the kinetically-controlled reaction rate is rapid. That is, if the reaction of the dimer species is larger, then the effect of the dispersion coefficient within the gel matrix is less than that of the overall chemical reaction rate in the mobile phase.

It appears that the kinetically-controlled rate between the mobile and stationary phases is, indeed, the principal determinant of the boundary profile in molecular sieve chromatography. In the section which follows, we describe the simulation of results for eqs. (13) and (15), as adapted to our computer flow diagram shown in fig. 1.

4.2. Evaluation of the partition coefficient

The values of the partition coefficients were calculated according to the equation $\sigma = \text{erfc}[(a - a_0)/b_0]$ [27,32], where a is the molecular radius and a_0 and b_0 are calibration constants defining the porosity of the gel. The error function complement is defined by

$$\text{erfc}(x) = \frac{2}{\pi^{1/2}} \int_x^\infty e^{-t^2} dt = 1 - \frac{2}{\pi^{1/2}} \int_0^x e^{-t^2} dt \,. \tag{30}$$

For Sephadex G200R gel, the partition coefficients shown in table 1 were used to calculate ξ_1, ξ_2, ξ_4, ξ_8. In our computer program, a single ratio was used, such as $\xi_1 : \xi_4 : \xi_8$. Values of α and β used were $\alpha = 0.295$ and $\beta = 0.67$ [13], where $\xi_i = \alpha + \beta\sigma_i$. The column cross-sectional area, A, was 1 cm^2.

4.3. Axial dispersion coefficients [23]

Axial dispersion coefficients for both solute species were calculated from the relationship

$$L_v = L_p + \frac{\xi D}{F} + \frac{qd^2F}{\xi^3 A^2 D} \,. \tag{31}$$

The term qd^2 relates the particle size and geometry to the average equilibrium time between mobile and stationary phases of the column. L_p results from the finite size of the gel particles and random variations in particle gel packing. In the present simulation, a value of 5.4×10^{-6} cm^2 was used for qd^2. D is the free diffusion coefficient of the interacting solute. Calculated values of L_i are given in table 2.

The equilibrium constants (in ml/mg) were chosen to give 10, 25, 50, 75 and 90% of the weight fraction of monomer, as shown in table 3.

4.4. The effect of gel particle size

It has been shown that the axial dispersion coefficient of an individual solute varies as the square of the gel diameter from eq. (31) [22]. Although the characteristics of the reaction boundary are known to be highly sensitive to variations in particle size, the sharpening of the boundary observed in figs. 3a, b must be attributed to the rapid rate of chemical equilibration and the kinetically-controlled rate of gel permeation between mobile and stationary phases, with only a minimal dependence on axial dispersion.

4.5. The effect of the kinetic reaction rates on monomer–tetramer association in the mobile and stationary phases

Fig. 4a shows our simulation of the concentration gradient profile for monomer–tetramer association, subject to gel chromatography on Sephadex G200R, using data from Zimmerman and Ackers [13]. The gradient curve shows a bimodal reaction boundary

($n > 2$) for monomer–n-mer systems in large-zone experiments. It is clear that our large zone experiments are an exacting duplication of the trailing boundaries of the concentration gradient profiles reported in earlier experiments [21–23], where $k_{ij} \geqslant 0.5\ \text{min}^{-1}$ as a function of the weight fraction of monomer at 120 minutes.

When the kinetic rate, k_{ij}, is varied for 0.0 to 0.5 min^{-1} in the mobile phase, using the first three steps of our schematic flow diagram (fig. 1), the pronounced effect of the kinetic reaction rate on the bimodality of the trailing edge of the boundary profile may be seen in figs. 4b and 4c. These figures are generated from curve 4 of fig. 4a by our computer simulation. In contrast, the plateau region of the leading edge remains relatively constant.

If the fitting of the simulated chromatographic profile to experimental data is to be used to determine the stoichiometry and equilibrium constants for a self-associating solute, the simulation of chemical equilibrium between the mobile and stationary phase must be considered.

The development of the reaction boundary as a function of column length is also influenced by the effective kinetic rate of local equilibration between mobile and stationary phases. Assuming that the rate of chemical equilibration in the mobile phase is very rapid ($k_{ij} \geqslant 0.5\ \text{min}^{-1}$), we have considered five sets of kinetic parameters in examining the rate of equilibration between the mobile and stationary phases.

A(1): $k_{11} = k_{44} = 1.0\ \text{min}^{-1}$, $k_{-11} = k_{-44} = 0.2\ \text{min}^{-1}$

In this case, k_{ii} is five times faster than k_{-ii}, hence k_{11}, the rate of reverse equilibration of the monomer from the gel matrix to the mobile phase, and k_{44}, that of the tetramer, are of similar magnitude. k_{-11} and k_{-44}, the rate of forward equilibration of monomer and tetramer from the mobile phase to the gel matrix, are also equal.

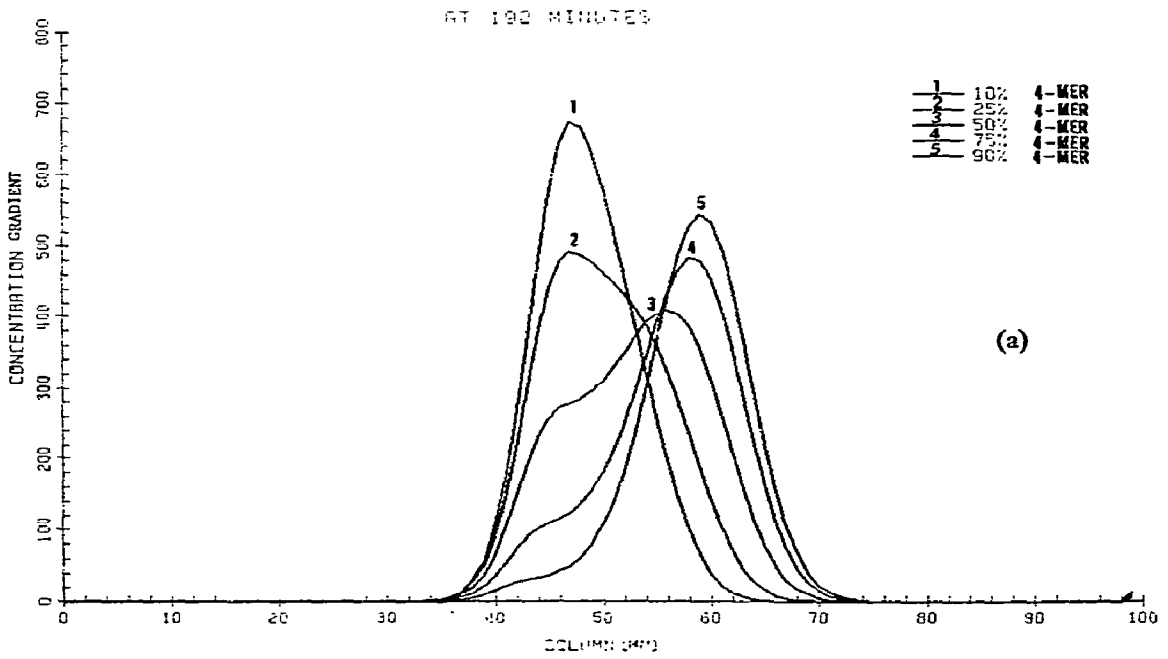

Fig. 4a. Simulated gel chromatography on Sephadex G200R of a rapidly equilibrating monomer–tetramer system, where $k_{ij} \geqslant 0.5\ \text{min}^{-1}$. Monomer has a molecular weight of 17000 daltons. Equilibrium constants are given in table 3. Column cross-sectional area = 1.0 cm^2. Flow rate is 1.2 ml/h, time = 192 min. 1. 10% tetramer, 2. 25% tetramer, 3. 50% tetramer, 4. 75% tetramer, 5. 90% tetramer.

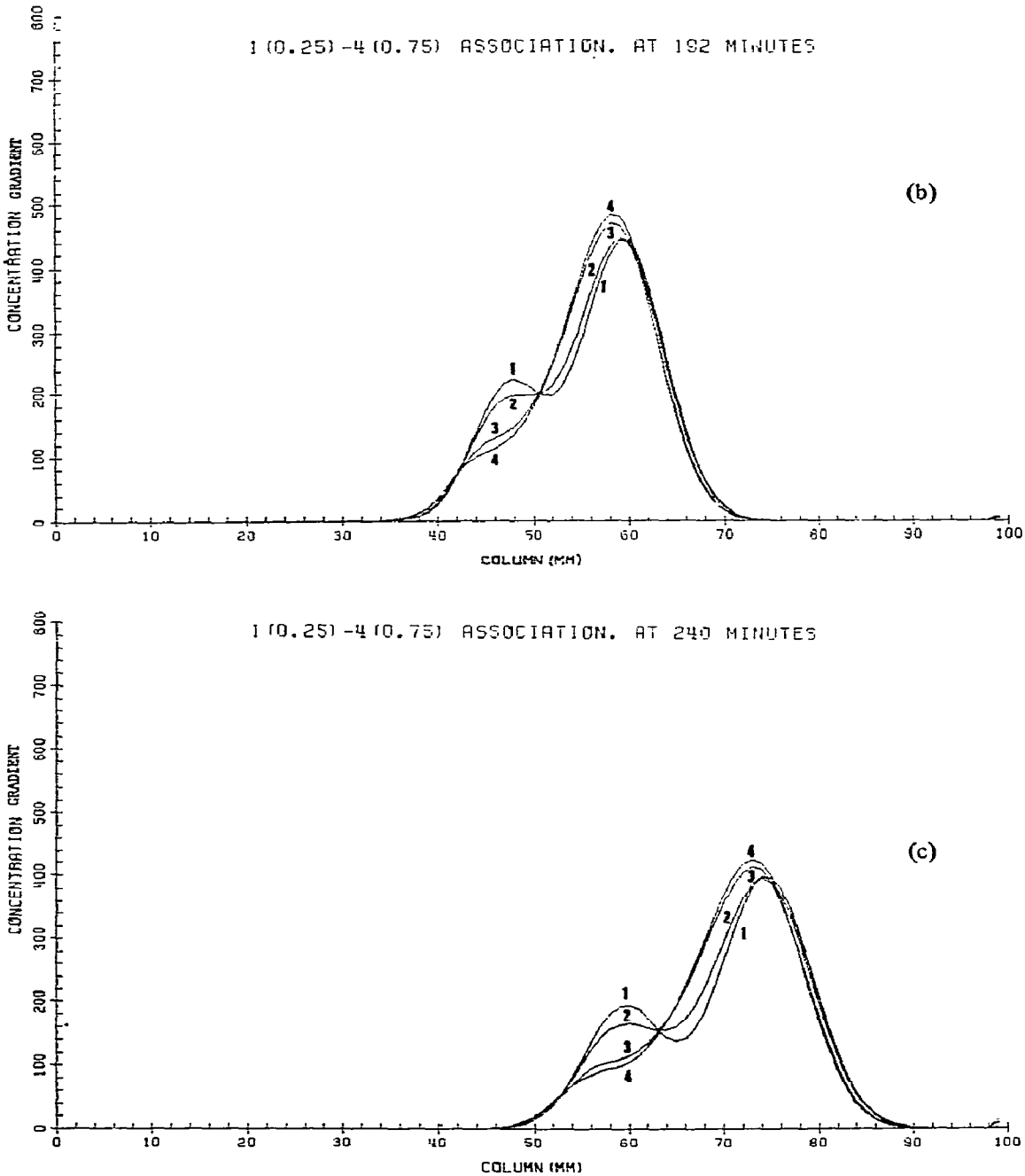

Fig. 4b, c. Simulated gel chromatography on Sephadex G200R of a monomer–tetramer system in a ratio of 25 : 75% as influenced by kinetically-controlled interaction in the mobile phase at (b) 192 min and (c) 240 min. 1. $k_{41} = 0.0$ min^{-1}, $k_{14} = 0.0$ min^{-1}. 2. $k_{41} = 0.005$ min^{-1}, $k_{14} = 0.005$ K$_4$ (min^{-1}). 3. $k_{41} = 0.05$ min^{-1}, $k_{14} = 0.05$ K$_4$ (min^{-1}). 4. $k_{41} \geq 0.5$ min^{-1}, $k_{14} \geq 0.5$ K$_4$ (min^{-1}).

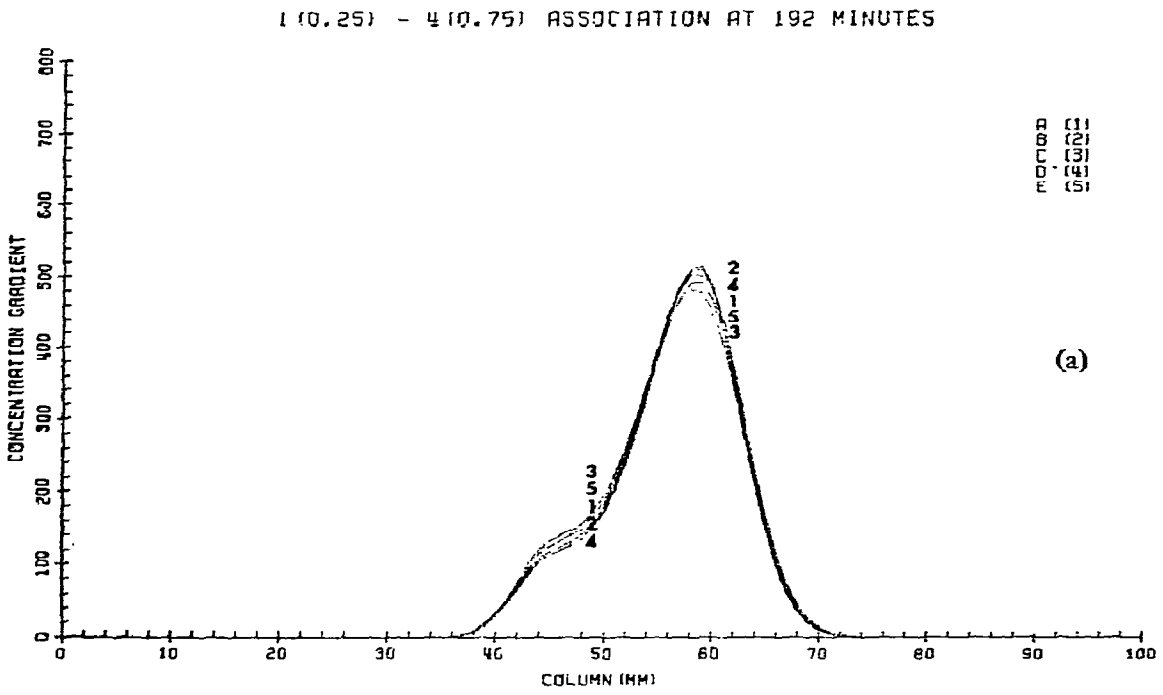
I (0.25) - 4 (0.75) ASSOCIATION AT 192 MINUTES
A (1)
B (2)
C (3)
D (4)
E (5)
CONCENTRATION GRADIENT
COLUMN (MM)
(a)

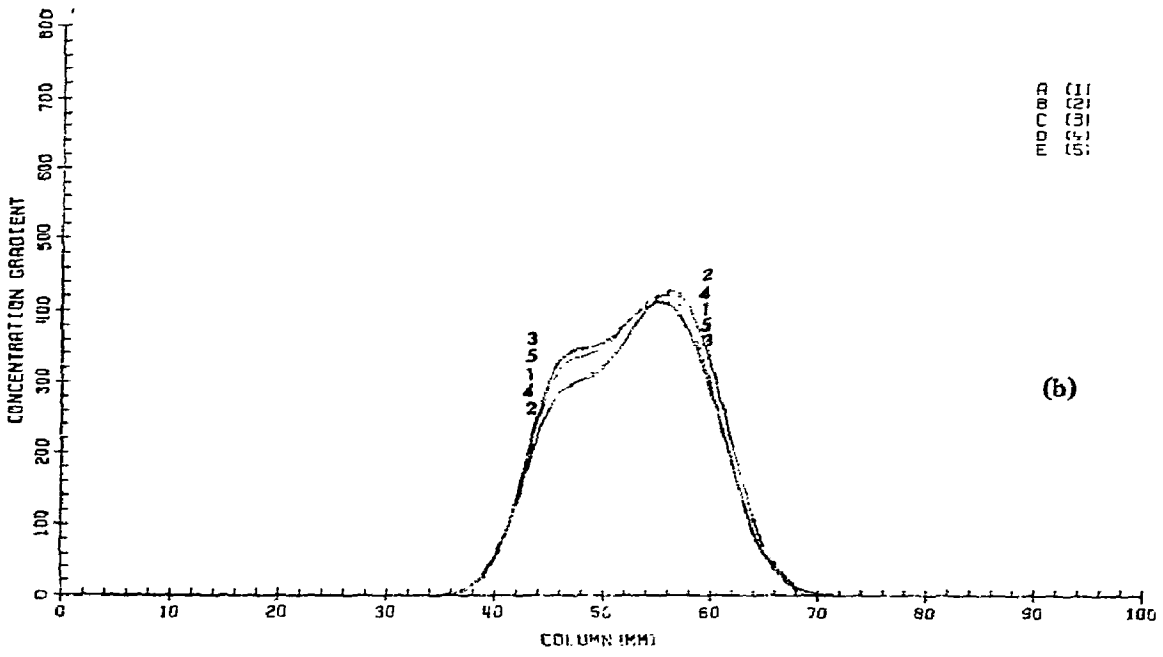
I (0.50) - 4 (0.50) ASSOCIATION AT 192 MINUTES
A (1)
B (2)
C (3)
D (4)
E (5)
CONCENTRATION GRADIENT
COLUMN (MM)
(b)

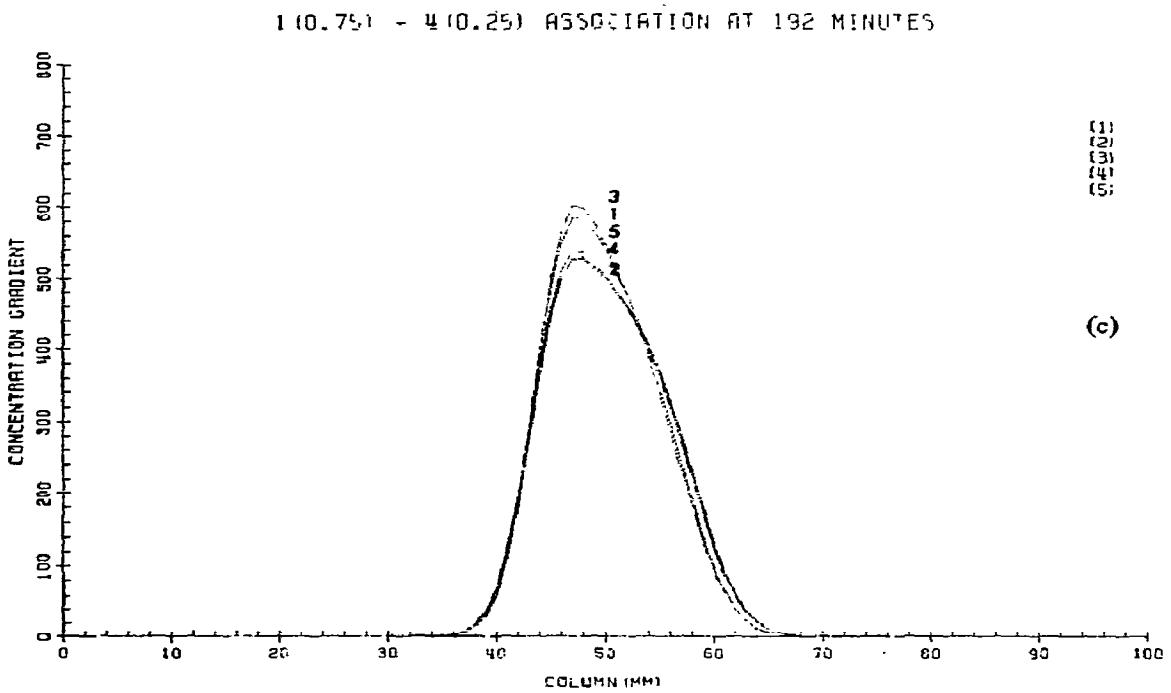

Fig. 5a, b, c. Simulated gel chromatography on Sephadex G200R of a monomer–tetramer system, considering all kinetic effects in the mobile and stationary phases, using the four-step flow diagram of fig. 1, at 192 min, where $k_{41} > 0.5$ min^{-1}, $k_{14} > 0.5$ K_2 (min^{-1}) in the mobile phase. A(1) $k_{11} = k_{44} = 1.0$ min^{-1}, $k_{-11} = k_{-44} = 0.2$ min^{-1}. B(2) $k_{11} = 1.0$ min^{-1}, $k_{-11} = 0.1$ min^{-1}; $k_{44} = 0.1$ min^{-1}, $k_{-44} = 0.02$ min^{-1}. C(3) $k_{11} = 0.1$ min^{-1}, $k_{-11} = 0.02$ min^{-1}; $k_{44} = 1.0$ min^{-1}, $k_{-44} = 0.1$ min^{-1}. D(4) $k_{11} = 0.1$ min^{-1}, $k_{-11} = 0.01$ min^{-1}; $k_{44} = 1.0$ min^{-1}, $k_{-44} = 0.2$ min^{-1}. E(5) $k_{11} = k_{44} = 0.1$ min^{-1}, $k_{-11} = k_{-44} = 0.1$ min^{-1}. (a) monomer–tetramer ratio of 25 : 75 of curve 4 of fig. 4a. (b) monomer–tetramer ratio of 50 : 50 of curve 3 of fig. 4a. (c) monomer–tetramer ratio of 75 : 25 of curve 2 of fig. 4a.

B(2): $k_{11} = 1.0$ min^{-1}, $k_{-11} = 0.1$ min^{-1};

$k_{44} = 0.1$ min^{-1}, $k_{-44} = 0.02$ min^{-1}.

Here k_{11} of the tetramer is ten times faster than k_{44}, and k_{-11} of the tetramer is five times faster than k_{-44}.

C(3): $k_{11} = 0.1$ min^{-1}, $k_{-11} = 0.02$ min^{-1};

$k_{44} = 1.0$ min^{-1}, $k_{-44} = 0.1$ min^{-1}.

In this case, k_{44} of the tetramer is ten times faster than k_{11}, and k_{-44} is twenty times faster than k_{-11}.

D(4): $k_{11} = 0.1$ min^{-1}, $k_{-11} = 0.01$ min^{-1};

$k_{44} = 1.0$ min^{-1}, $k_{-44} = 0.2$ min^{-1}.

Here, k_{44} of the tetramer is ten times faster than k_{11}, and k_{-44} is twenty times faster than k_{-11}.

E(5): $k_{11} = k_{44} = 1.0$ min^{-1}, $k_{-11} = k_{-44} = 0.1$ min^{-1}.

In this final case, k_{11} and k_{44} are both ten times faster than k_{-11} and k_{-44}.

The time course dependent simulation of the concentration gradient profile for monomer–tetramer association on Sephadex G200R is shown in figs. 5a, b, and c, using the computer schematic of fig. 1, considering the parameters of cases A(1) through E(5) and varying the weight fraction of monomer. In each of the resulting boundary profiles, there are distinct regions where kinetic controls are evident, indicated here by numerals. We found, however, in the region where the parameters $k_{11} = k_{-11} < 0.01$ min^{-1} and $k_{44} = k_{-44} < 0.01$ min^{-1} are assumed, no kinetic controls

are evident in the boundary profiles.

An overview of the effect of kinetic controls on the boundary profile may be seen where figs. 4a, 4b and 5a are compared. When curve 4 of fig. 4a (from Zimmerman and Acker's data [13]) is compared with fig. 4b and 5b, it is apparent that (1) decreasing the rate of chemical equilibration in the mobile phase has a major effect on the shape of the profile, (2) slow rates of equilibration of monomer and tetramer between mobile and stationary phases have a relatively small effect on the shape of the profile and (3) slow rates of equilibration between the two phases have an effect similar to that of decreasing the rate of chemical equilibration about ten-fold from $k_{41} \geq 0.5\ \text{min}^{-1}$ to $k_{41} = 0.05\ \text{min}^{-1}$. Hence in practice, it becomes difficult to distinguish between the two processes under these conditions.

4.6. Simulation of monomer–tetramer–octomer association

Simulation of cases of three-species association is based on eq. (13), where each compartment of the first three sections 0. 1, 2 or the schematic flow diagram (fig. 1) consists of three species.

Computer simulation was limited to consideration of the mobile phase, due to the complexity of dealing with three-species association in both the mobile and stationary phases. Application of our computer program for evaluation of boundary profile will be described in detail in a succeeding paper.

Development of the reaction boundary as a function of column length, varying the kinetic constant from 0.0 to 0.5 min^{-1} on Sephadex G200R is shown in figs. 6a, b, and c. As may be seen from these figures, the resulting reaction is bimodal, unless one considers an ideal system in which no kinetic effects are assumed, in which case a trimodal reaction boundary is observed. This is consistent with findings reported by Zimmerman [21].

5. Conclusion

Our findings indicate that while the chemical reaction rate in the mobile phase is the principal determinant of the shape of the elution boundary, the kinetically controlled reaction rate between the mo-

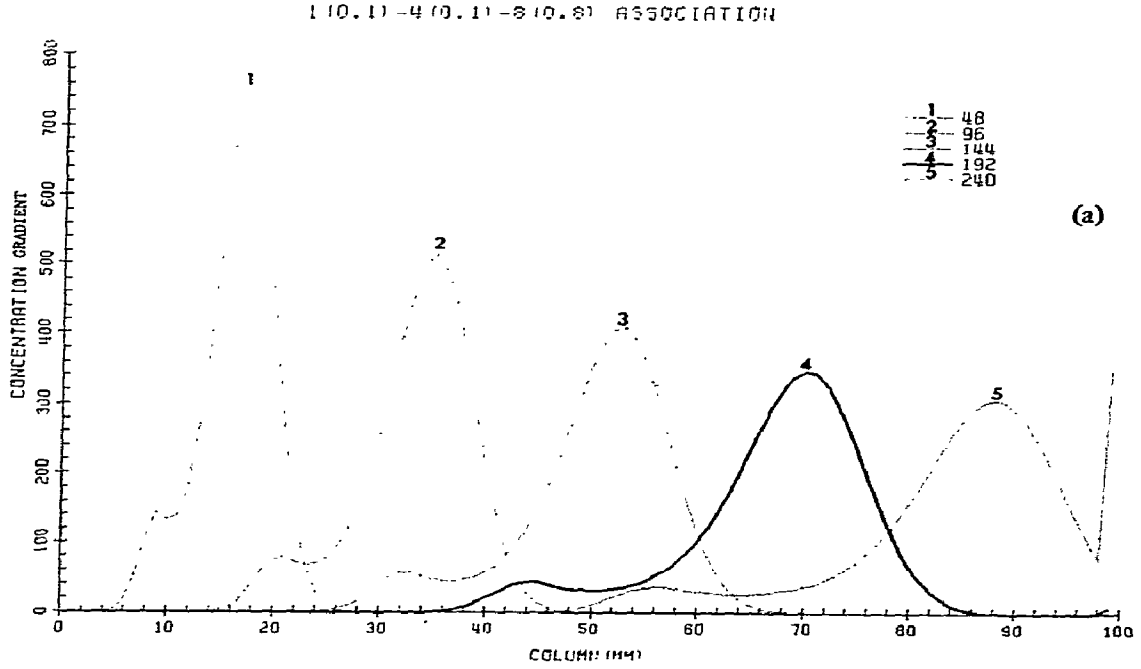

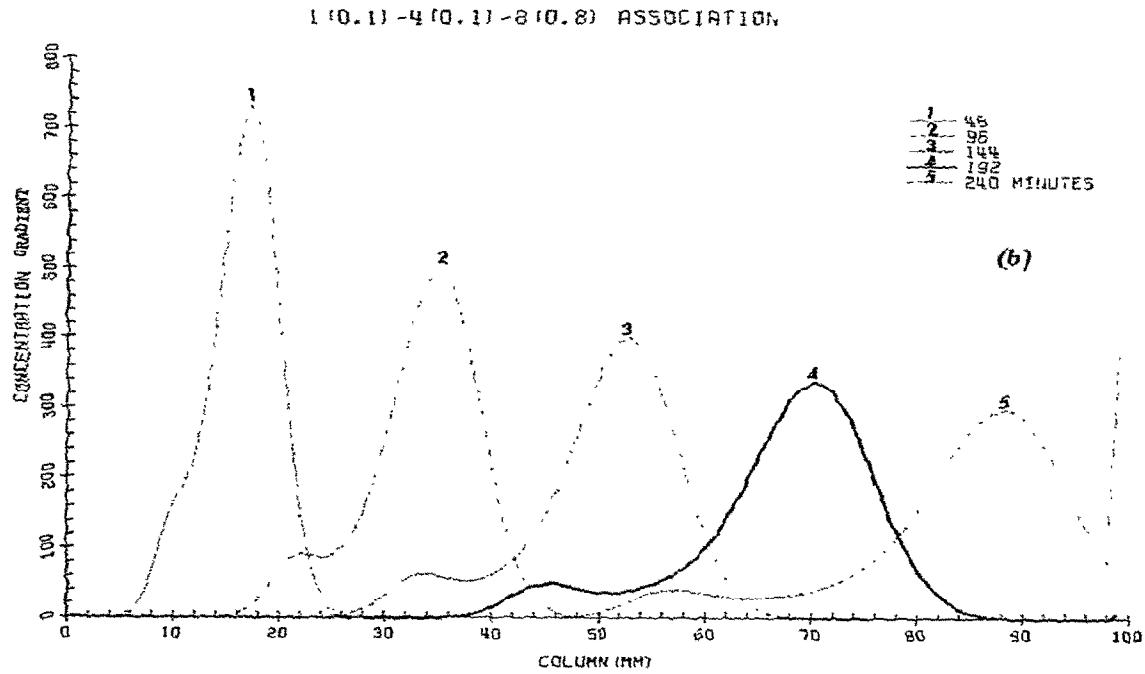
1(0.1)-4(0.1)-8(0.8) ASSOCIATION
CONCENTRATION GRADIENT
COLUMN (MM)
1 48
2 96
3 144
4 192
5 240 MINUTES
(b)

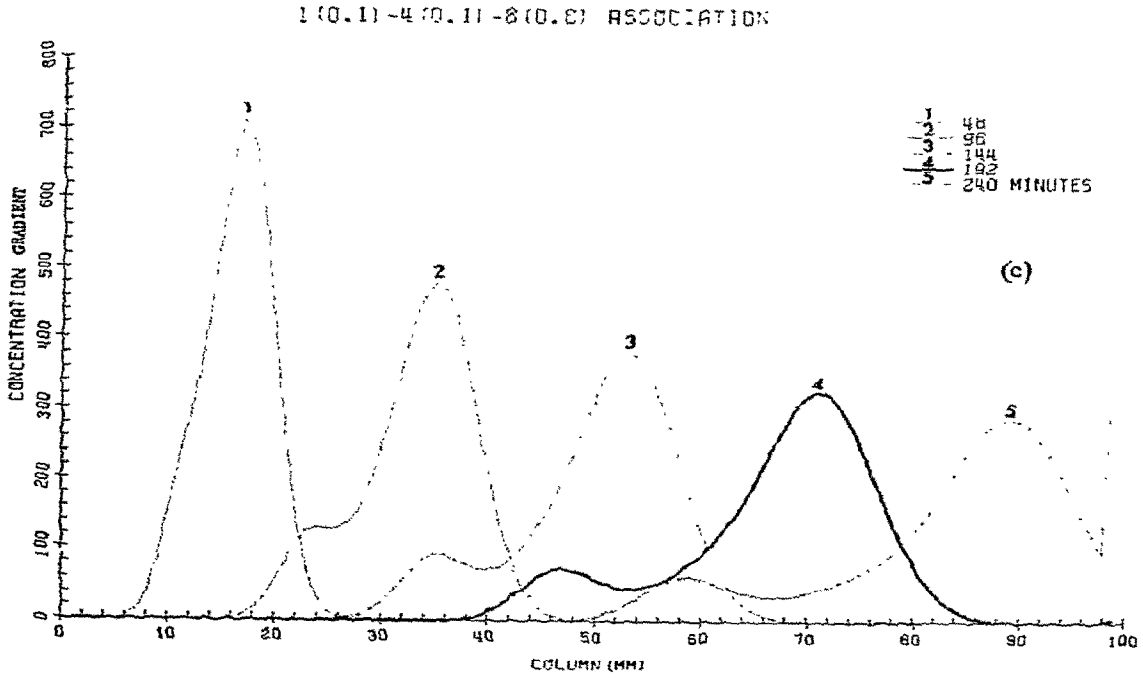
1(0.1)-4(0.1)-8(0.8) ASSOCIATION
CONCENTRATION GRADIENT
COLUMN (MM)
1 48
2 96
3 144
4 192
5 240 MINUTES
(c)

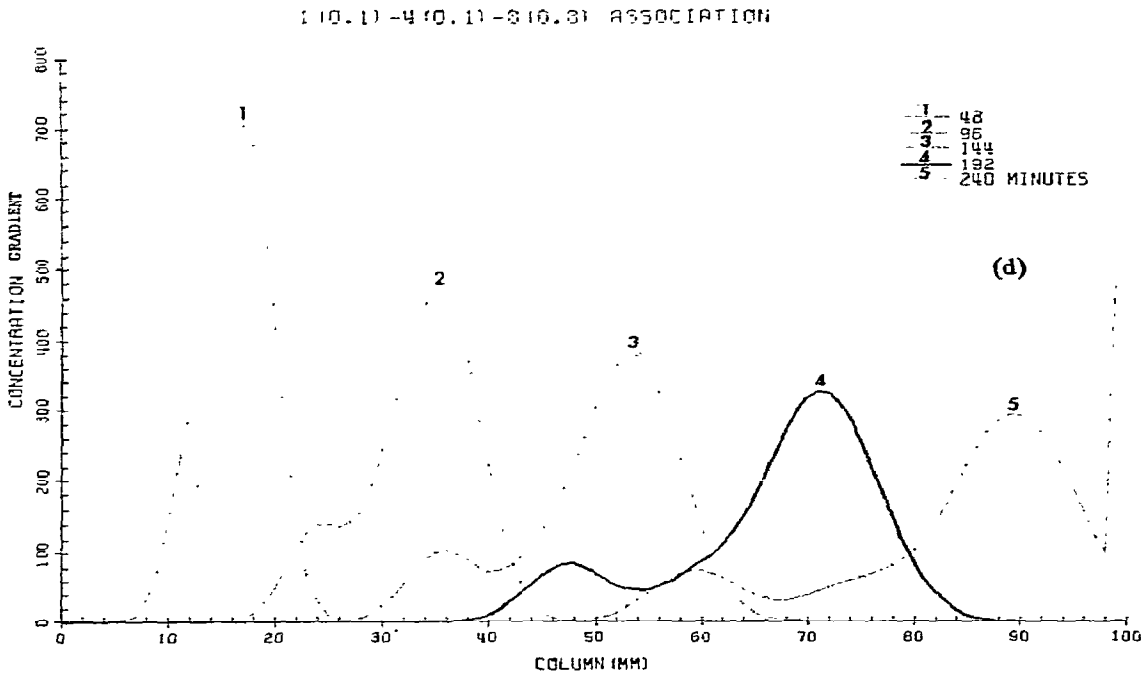

Fig. 6a, b, c, d, Simulated gel chromatography on Sephadex G200R of the mobile phase of monomer–tetramer–octamer system in the ratio of 10 : −10 : 80 as a function of elution time. (1) 48 min, (2) 144 min, (3) 192 min, (4) 240 min. (a) $k_{81} > 0.5$ min^{-1}, $k_{41} > 0.5$ min^{-1}, $k_{18} > 0.5$ K$_8$(min^{-1}), $k_{14} > 0.5$ K$_4$(min^{-1}). (b) $k_{81} = 0.05$ min^{-1}, $k_{41} = 0.05$ min^{-1}, $k_{18} = 0.05$ K$_8$ (min^{-1}), $k_{14} = 0.05$ K$_4$(min^{-1}). (c) $k_{81} = 0.005$ min^{-1}, $k_{41} = 0.005$ min^{-1}, $k_{18} = 0.005$ K$_8$(min^{-1}), $k_{14} = 0.005$ K$_4$(min^{-1}). (d) no interaction, $k_{81} = k_{18} = 0.0$ min^{-1}, k_{41} and $k_{14} = 0.0$ min^{-1}.

bile and stationary phases is the principal perturbing factor of the reaction boundary. Hence, decreasing the rate of equilibration in the mobile phase has a much greater effect on the shape of the boundary profile in molecular sieve chromatography than does decreasing the rate of equilibration between phases.

The most significant overall finding of these computer-simulated gel permeation experiments is that the kinetically-controlled effects of local equilibration in either the mobile or stationary phase must be considered in evaluating the elution boundary profiles. Further investigation is required to elucidate the nature and extent of such kinetic effects on the interaction of self-associating solutes undergoing rapid equilibration. Schematically, this interaction might possibly be shown as

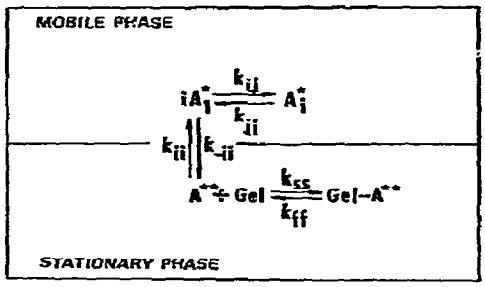

assuming that the reversible binding of the solute to the gel matrix in the stationary phase contributes significantly to the effective rate of isomerization between the mobile and stationary phases.

Since the column equilibration coefficient is not

always constant for a given interacting species in such a system, the apparent equilibrium constant should vary as a function of the distance coordinate. The concentration gradient profiles should vary when evaluated for each species at each point along the column between the mobile and stationary phases [33].

In considering a case of monomer–dimer association, shown in this figure, in which the weight fraction of monomer at equilibrium concentration is 50 : 50, instantaneous equilibration is represented by curve 1, plotting weight fractions versus equilibration time, where $k_{ij} \geqslant 0.5\ \text{min}^{-1}$. A plot of the concentration of monomer, where $k_{ij} < 0.5\ \text{min}^{-1}$, decreases exponentially along curve 2. At the same time, the concentration of dimer increases along curve 3. The difference between these two curves gives $t_{1/2}$, the shaded area shown in the figure.

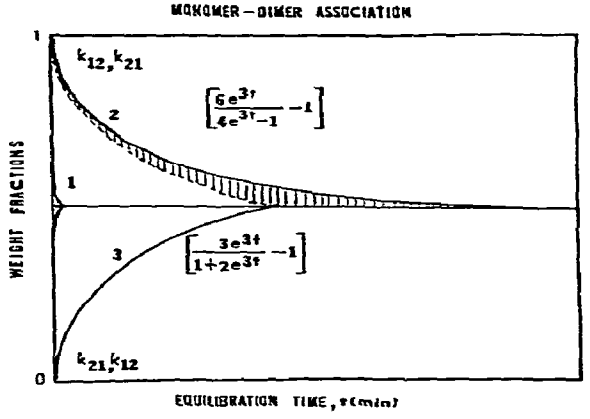

Ideally, one would expect the concentrations of both monomer and dimer to reach a 50 : 50 equilibrium concentration at every point along the column. Such ideal behavior, however, does not take into consideration the kinetic effect on the interaction of self-associating solutes. In fact, when the weight fraction of dimer reaches 50%, the magnitude of $t_{1/2}$ of monomer is twice that of dimer. Therefore, we may assume that the rate of equilibration of this reaction is kinetically controlled, but that the kinetic effect varies with the distribution of each species along the column, i.e. $dK/dx \neq 0$ [36].

Acknowledgement

The authors wish to express their thanks to Dr. Gary K. Ackers for his critical review and suggestions in the preparation of this manuscript.

References

[1] G.A. Gilbert, Discussion Faraday Soc. 20 (1955) 68.
[2] G.A. Gilbert and R.C.L. Jenkins, Proc. Roy. Soc. A253 (1959) 420.
[3] G.K. Ackers and T.E. Thompson, Proc. Natl. Acad. Sci. 53 (1965) 342.
[4] D.J. Cox, Arch. Biochem. Biophys. 112 (1965) 249, 259
[5] D.J. Cox, Arch. Biochem. Biophys. 119 (1967) 230.
[6] D.J. Cox, Arch. Biochem. Biophys. 129 (1969) 106.
[7] D.J. Cox, Arch. Biochem. Biophys. 142 (1971) 514.
[8] J.R. Cann and W.B. Goad, J. Biol. Chem. 240 (1965) 148.
[9] J.R. Cann and W.B. Goad, Arch. Biochem. Biophys. 153 (1972) 603.
[10] J.R. Cann, Interacting molecules (Academic Press, New York, 1970).
[11] L.W. Nichol and D.J. Winzor, Migration of interacting systems (Clarendon Press, Oxford, 1972).
[12] J.R. Cann and D.C. Oates, Biochemistry 12 (1973) 1112
[13] J.K. Zimmerman and G.K. Ackers, J. Biol. Chem. 246 (1971) 1078.
[14] J.K. Zimmerman and G.K. Ackers, J. Biol. Chem. 246 (1971) 7289.
[15] J.K. Zimmerman, D.J. Cox and G.K. Ackers, J. Biol. Chem. 246 (1971) 4242.
[16] J.K. Zimmerman and G.K. Ackers, Anal. Biochem. 57 (1974) 578.
[17] G.G. Belford and R.L. Belford, J. Chem. Phys. 17 (1962 1926.
[18] K.E. van Holde, J. Chem. Phys. 37 (1962) 1922.
[19] J.R. Cann and G. Kegeles, G. Biochem. 13 (1974) 1868.
[20] J.K. Zimmerman, Biochem. 13 (1974) 384.
[21] J.K. Zimmerman, Biophysical Chem. 3 (1975) 339.
[22] J.R. Cann, Biophysical Chem. 1 (1973) 1.
[23] H.R. Halvorson and G.K. Ackers, J. Biol. Chem. 249 (1974) 967.
[24] G.K. Ackers, Adv. Prot. Chem. 24 (1970) 343.
[25] D.F. Overhauser, J.L. Bethune and G. Kegeles, Biochemistry 4 (1965) 1878.
[26] G.H. Weiss and G.K. Ackers, Biopolymers 11 (1972) 2125.
[27] G.K. Ackers, J. Biol. Chem. 242 (1967) 3026, 3237.
[28] J.C. Gidding, J. Phys. Chem. 68 (1964) 184.
[29] L.J. Gosting, Advan. Prot. Chem. 11 (1956) 429.
[30] H. Vink, Acta Chem. Scad. 18 (1956) 429.
[31] H.R. Halvorson and G.K. Ackers, J. Poly. Sci. Part H2, 9 (1971) 9.
[32] G.K. Ackers, J. Biol. Chem. 243 (1968) 2056.
[33] P.W. Chun and M.C.K. Yang, (unpublished results) (1977).
[34] H. Schönert, Biophys. Chem. 3 (1975) 161.
[35] R.M. Mitchell, Biopolymers 15 (1976) 1717, 1741.
[36] P.W. Chun and Y.J. Yoon, Biopolymers, in press (1977).
[37] P.W. Chun, Biophys. Chem. 2 (1974) 170.